Scientific Research Publishing

World Journal of Mechanics, 2024, 14, 143-168
https://www.scirp.org/journal/wjm
ISSN Online: 2160-0503
ISSN Print: 2160-049X

# Experimental Procedure and Hardening Model to Consider Forming and Baking Effects in Simulation

**Jiho Lim*, Haea Lee, Jisik Choi**

POSCO, Incheon, Republic of Korea
Email: *jiholim@posco.com

**How to cite this paper:** Lim, J.H., Lee, H.A. and Choi, J.S. (2024) Experimental Procedure and Hardening Model to Consider Forming and Baking Effects in Simulation. *World Journal of Mechanics*, **14**, 143-168.
https://doi.org/10.4236/wjm.2024.147007

**Received:** June 29, 2024
**Accepted:** July 28, 2024
**Published:** July 31, 2024



## Abstract

This paper investigated an experimental method for bake hardening properties, a technique for deriving the true stress-strain curves after reaching the maximum load, and a constitutive equation considering both work hardening and bake hardening in order to apply the work hardening occurring in the forming process of parts and the bake hardening induced in the baking process to an automotive crash simulation. A general bake hardening test is that a pre-tensioned specimen is baked and then the same specimen is tensioned again without any further treatment. For a bake hardening test of automotive steel with a tensile strength of 1.2 GPa or more, fractures often occur in curvature section outside, an extensometer due to the difference in the material strength caused by non-uniform bake hardening. This causes a problem in that the bake hardening properties cannot be obtained. In this paper, to prevent curvature fracture, tensile specimens were re-machined in the uniformly deformed region of large specimens subjected to pre-strain, and the re-machined specimens with uniform strength in all regions were re-tensioned. In the bake hardening test of ultra-high strength steels with a tensile strength of 1 GPa or more, shear band fractures occur when the pre-strain is large. This makes it impossible to obtain a true stress-strain curve because there is no uniformly deformed region under a tensile test. To overcome this problem, a new method to calculate the true stress-strain curve by comparing experimental results and the load calculated by the local strain obtained from digital images was developed. This method can be applied not only where shear band deformation occurs, but also in necking deformation, and true stress-strain curves for strains up to 2 - 3 times the uniform elongation can be obtained. A new constitutive equation was developed since an appropriate hardening model is required to simultaneously apply the work hardening and the bake hardening to the simulation. For the newly developed model, the user material subroutine of LS-Dyna was configured,

and the simulation was performed on the single hat specimens with pre-strain. When both work hardening and bake hardening were considered, there was a significant increase in absorbed energy compared to when only work hardening was considered. This means that both work hardening and bake hardening should be considered in the car crash simulations to enhance the accuracy of the simulation.

## Keywords

Bake Hardening, Hardening Model, Digital Image Correlation (DIC), Inverse Method, Ultra High Strength Steel (UHSS)

## 1. Introduction

An automotive body is manufactured by assembling parts made by forming and going through a painting process. The strength of automotive steel used in automotive bodies usually increases due to work hardening in the forming process and baking hardening in the painting process. Therefore, the actual assembled automotive parts are stronger than the original materials due to the combined effects of work hardening and bake hardening. However, the material properties of original material without considering the forming and painting processes have usually been applied to car crash simulations, so the difference in material properties between real parts and simulation models can act as a factor of error in predicting the crash performance during a car design process.

The main mechanism of the bake hardening is related to the Cottrell atmosphere. Cottrell atmosphere involves the interaction between the mobile dislocations and the interstitial atoms, such as carbon inside the ferrite grains. Thus, the bake hardening depends mainly on the density of the mobile dislocations and the dissolved carbon atoms [1]. Ramazani *et al.* [2] studied the changes in mechanical properties such as yield stress, tensile strength and elongation according to the pre-strain for DP600 and TRIP700 steels, and clarified that mechanical properties were related to microstructural features. Soliman *et al.* [3] studied tensile properties and strain aging behavior of ferrite-martensite dual-phase steels and concluded that pre-straining was a decisive factor for the BH response. Chaurasiya *et al.* [4] investigated the effect of 0% - 10% pre-strain on the tensile behavior of HS800 steel. Robertson *et al.* [5] studied the effect of pre-strain and bake hardening on the fatigue properties of TRIP steel. Pereloma *et al.* [6] investigated the effect of pre-strain and bake hardening on the microstructure of TRIP steel. Recently, the Ultra High Strength Steel (UHSS) with the tensile strength of 1 GPa or more such as DP, TRIP and martensitic steels has recently been used widely to reduce the weight of an automotive body. UHSS has a high carbon content for high strength, so its bake hardening is superior to conventional steels. Therefore, it is necessary to consider the change of material properties due to work hardening and bake hardening in crash analysis.

In order to consider the material properties due to the pre-strain and baking in

the crash simulation, it is necessary to derive the stress-strain curve after maximum load. Generally, the stress-strain curve after reaching the maximum load cannot be directly calculated using formulas from experimental data, so indirect methods are used. Since the bulge test can obtain the stress-strain curve up to larger strain than the tensile test, the bulge test can be used to convert the stress-strain curve into tensile stress-strain curve based on the principle of equivalent plastic work. Stoughton *et al.* [7] used a method to obtain the stress-strain curve through numerical analysis of the relationship between true stress and strain on the surface of a tensile specimen by the DIC (Digital Image Correlation) system. This method has the limitations that the strain is uniform in the width direction of the specimen and the difference between the stress in longitudinal direction and the von Mises stress is not large. Coppieters *et al.* [8] identified the post-necking hardening by the comparison of the internal and external work in the necking zone. Zhao *et al.* [9] proposed a method for obtaining the flow curve over large strain through the combination of test and finite element analyses. Capilla *et al.* [10] proposed an approach to determining the large-strain flow curve of sheet metals by using in-plane stretch-bending test data.

Many researchers have studied to consider the bake hardening effect in the simulation. Ballarin *et al.* [11] proposed a formula expressing bake hardening as the sum of the Cottrel effect and the precipitation effect. Durrenberger *et al.* [12] proposed a material model according to pre-strain and bake hardening and verified the analysis by applying the material model with an axial test of a hat specimen. Schwab *et al.* [13] explained that the upper yield point generated by yield point elongation is larger than the observed value and the lower yield point is smaller than the observed value. Riemensperger [14] and Koch *et al.* [15] applied the method of shifting the work hardening curve by the increase in strength due to bake hardening in the simulation. Thuillier *et al.* [16] proposed an empirical work hardening model that expresses the yield function as the sum of the stress of the base material and overstress due to baking.

This paper aims to develop bake hardening test method and a hardening model related to the material properties required to simultaneously consider the work hardening in forming process and the bake hardening in painting process in crash simulation. A testing method was developed to suppress the fracture in the curvature of the tensile specimen, and a DIC inverse method was developed to obtain the stress-strain curve after reaching the maximum load even for non-uniform strain distribution using the local strain obtained from the DIC system. In order to apply the material properties obtained in the experiment to the simulation, a novel work hardening model considering work hardening and bake hardening was developed and verified by LS-Dyna user material subroutine.

## 2. Tensile Properties after Baking According to the Pre-Strain

### 2.1. Test Method for Bake Hardening Property

The bake hardening index of ASTM standard (ASTM A653) is defined as the

increase of material strength for the pre-strain after baking a pre-strained specimen and then re-tensioning it. The typical bake hardening test is that pre-straining ASTM tensile specimens are baked and then re-tensioned without any further treatment. The baking condition is heating at 170˚C for 20 minutes. The bake hardening generally increases as the pre-strain increases, and in particular, UHSS with the tensile strength of 1 GPa or more has a large increase in the yield stress as the yield point elongation occurs. For example, the 980DP steel in Figure 1 has the largest upper yield stress in the engineering stress-strain curve when the pre-strain is 2% or more.

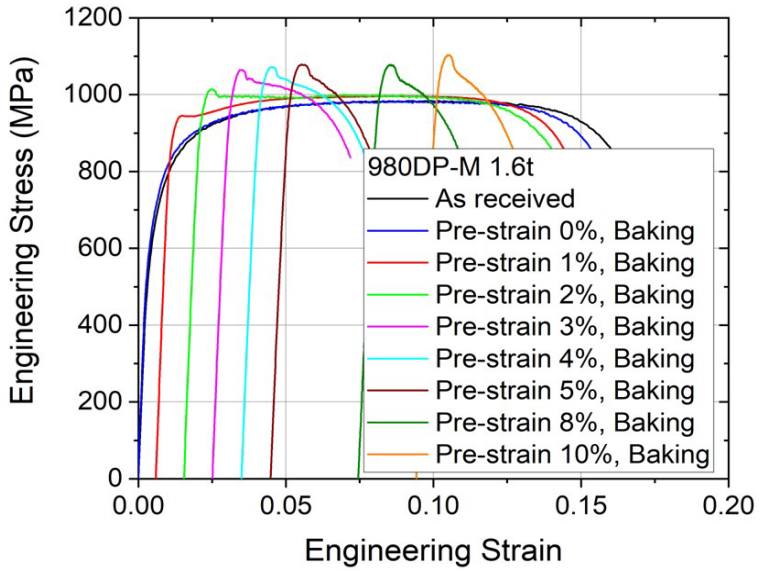


**Figure 1.** Engineering stress-strain curves of 980DP steel after baking according to pre-strain.

At the beginning of the tensile test, deformation of the tensile specimen starts at the intersection of the curvature and parallel regions due to stress concentration. The deformation gradually propagates to the center of the specimen due to work hardening. The tensile specimen undergoes uniform deformation on the inside of the extensometer, but the strain in the curvature region and grips gradually decreases as the width of the specimen increases. When the pre-strained specimen is baked, the material strength in the curvature region becomes lower than that in the parallel region due to low bake hardening. For a material with low elongation and high bake hardening, the deformation may concentrate on the intersection and fracture occurs outside the extensometer, as shown in Figure 2, before propagating to the parallel region. In this case, the strain cannot be measured with the extensometer, so the tensile properties of the material cannot be measured with the tensile test, as shown in Figure 3.

This is because the uneven deformation of parallel and curvature regions of the specimen causes a difference in the material strength after baking. In this paper, in order to eliminate the non-uniformity of material strength after baking, predeformation is applied to a KS-1B specimen with a parallel length of 220 mm, as

shown in Figure 4, and an ASTM tensile specimen re-machined in parallel section of KS-1B specimen is re-tensioned according to ASTM standard. When done this way, the fracture of the curvature region is significantly improved, as shown in Figure 5.

## 2.2. Calculation of Strain and Stress of Re-Tension Specimen Considering Pre-Strain

To calculate the stress after a test, the force is divided by the cross-sectional area of the specimen based on initial dimensions before pre-deformation. However,

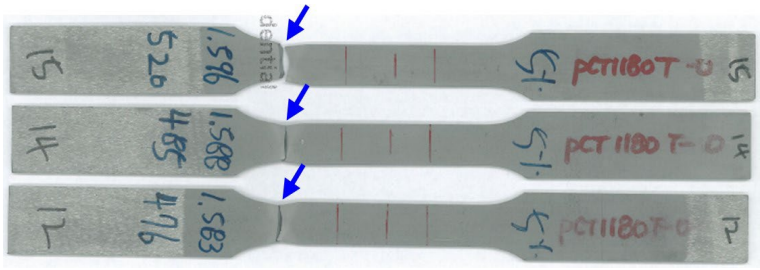

Figure 2. Deformed shape after failure of ASTM specimens of 1180 TRIP with 5% pre-strain and baking.

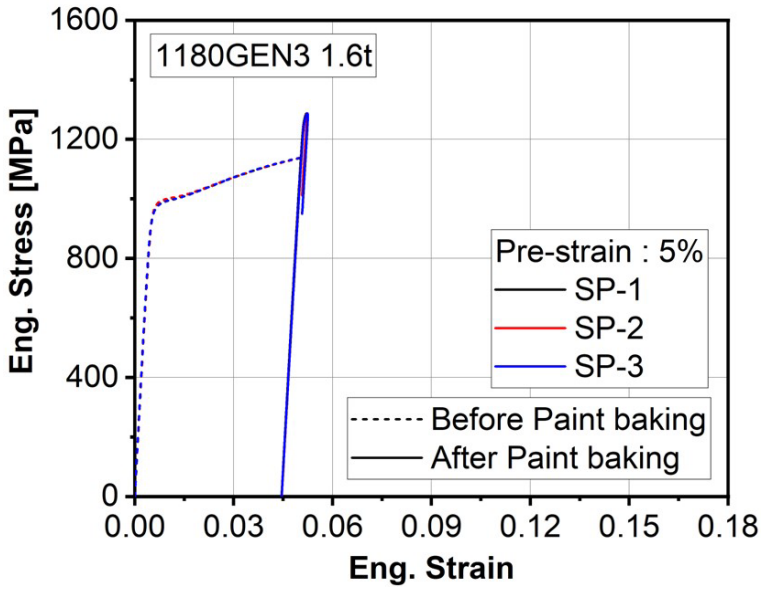


Figure 3. Engineering stress-strain curves of ASTM specimens with 5% pre-strain and baking.

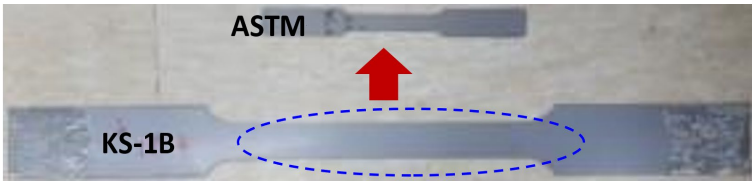


Figure 4. ASTM specimen re-machined from KS-1B specimen with pre-strain and baking.

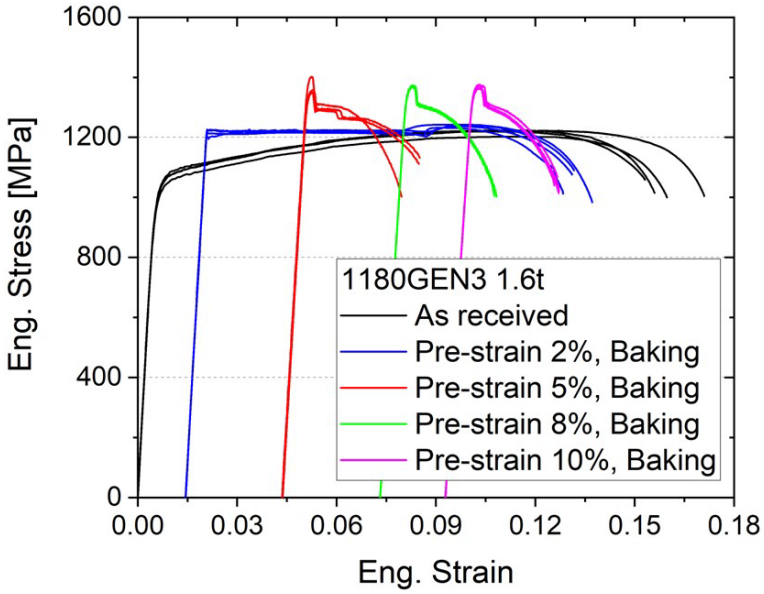


**Figure 5.** Engineering stress-strain curves for re-machined specimens of 1180GEN3 steel.

since the testing method in this paper is re-machining the specimen after pre-deformation, it is not possible to directly measure the width of the re-machined ASTM tensile specimen before pre-deformation. It can be assumed that the specimen is deformed at the same rate in the width and thickness direction. Therefore, the width of the re-machined ASTM specimen before pre-deformation in **Figure 6** can be calculated with a simple proportional formula, as shown in Equation (1).

$$w_0 = w_1 \times \frac{W_0}{W_1} \tag{1}$$

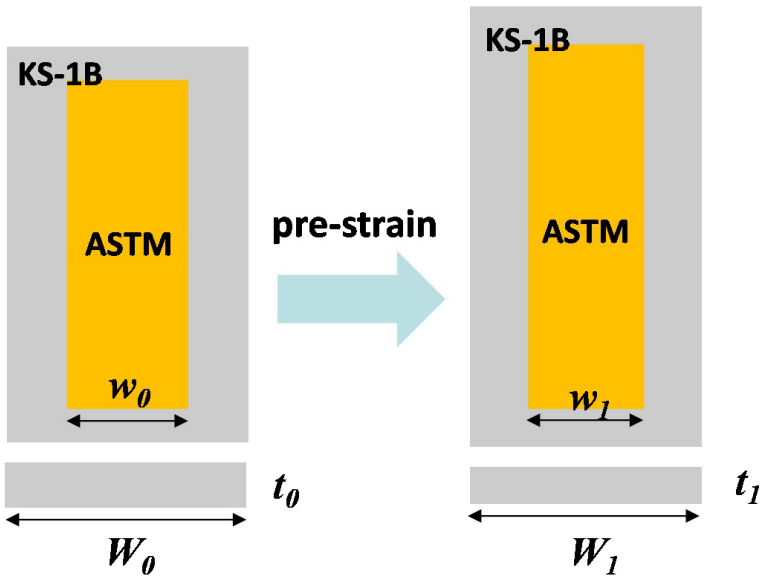


**Figure 6.** Schematic diagram of shapes of KS-1B and ASTM specimens before and after pre-deformation.

The relationship between the gauge section of the pre-tension specimen and the re-tension specimen is as shown in Figure 7. The pre-tension specimen with the gauge length of $L_0$ has a plastic deformation of $\Delta L_{0,p}$ remaining after the load is removed after the pre-tension of $\Delta L_0$. The gauge length, $L_1$, of the re-machined specimen, is composed of the original gauge section $L_0'$ and the plastic deformation $\Delta L_{0,p}'$ by the pre-tension. The strain measured by the DIC in the re-tension is the true strain for the deformation $\Delta L_1$ of re-tension based on the gauge length $L_1$ of re-tension specimen. That is, the strain measured by the DIC system in the tensile test of the re-machined ASTM specimen is the value calculated by assuming that the initial strain of the re-machined specimen after pre-tension is 0 even if there is pre-strain by pre-tension because the DIC system calculates by assuming that the strain of the specimen is 0 before testing. The actual true strain should be calculated using the length of non-deformed region, $\Delta L_0'$ as the gauge length. Therefore, it is necessary to analyze the relationship between the total strain and the strain measured by DIC, and adjust the strain based on the original state without pre-tension.

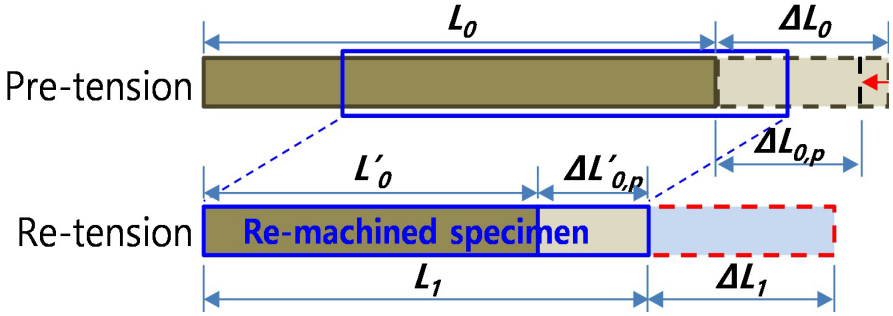


Figure 7. Schematic diagram for the relationship between the gauge sections of the pre-tensioned and the re-tensioned specimens.

When the load is removed after the pre-tension, the plastic strain ( $\varepsilon_{BH}^{p}$ ) is calculated as the engineering strain of the pre-tension ( $\varepsilon_{eng,BH}$ ) and the engineering stress ( $S_{BH}$ ) by Equation (2). And, the engineering strain after removing the pre-tension load ( $\varepsilon_{eng,BH}^{p}$ ) is calculated by Equation (3). In addition, the gauge length of the pre-tension specimen ( $L_0$ ), the length change by the pre-tension ( $\Delta L_0$ ), the plastic deformation after pre-tension ( $\Delta L_{0,p}$ ), the gage length of the re-machined specimen ( $L_1$ ), the length non-deformed part in the re-machined specimen ( $L_0'$ ) and the permanent deformed length in the re-machined specimen ( $\Delta L_{0,p}'$ ) have the relationship as Equations (4) and (5).

$$\begin{aligned}\varepsilon_{BH}^{p} &= \varepsilon_{BH} - \frac{\sigma_{BH}}{E} = \varepsilon_{BH} - \frac{S_{BH}\mathrm{e}^{\varepsilon_{BH}-\frac{1-2\nu}{E}\sigma_{BH}}}{E} \\ &\approx \ln\left(1+\varepsilon_{eng,BH}\right) - \frac{S_{BH}\left(1+\varepsilon_{eng,BH}\right)}{E}\end{aligned} \tag{2}$$

$$\varepsilon_{eng,BH}^{p} = \mathrm{e}^{\varepsilon_{BH}^{p}} - 1 = \left(1+\varepsilon_{eng,BH}\right)\mathrm{e}^{-\frac{S_{BH}\left(1+\varepsilon_{eng,BH}\right)}{E}} - 1 \tag{3}$$

$$\varepsilon_{eng,BH}^{p} = \frac{\Delta L_{0,p}}{L_0} = \frac{\Delta L'_{0,p}}{L'_0} \tag{4}$$

$$L'_0 = \frac{L_1}{L_0 + \Delta L_{0,p}} L_0 \tag{5}$$

The true strain ( $\varepsilon_m$ ) measured by the DIC system in the re-tension of the re-machined specimen is expressed as Equations (6) and (7).

$$\varepsilon_m = \ln\left(1 + \frac{\Delta L_1}{L_1}\right) \tag{6}$$

$$e^{\varepsilon_m} = 1 + \frac{\Delta L_1}{L_1} \tag{7}$$

The engineering strain ( $\varepsilon_{eng,T}$ ) of the re-tension for the state before pre-deformation is expressed by Equation (8). Substituting Equations (3)-(5) into Equation (7) gives equation (9). Substituting Equations (3) and (7) into Equation (9) produces Equation (10). And the true strain ( $\varepsilon_T$ ) for the state before pre-deformation is expressed as Equation (11). As a result, the true strain ( $\varepsilon_T$ ) is the sum of the plastic strain due to pre-strain and the strain ( $\varepsilon_m$ ) measured by the DIC system in re-tension. In addition, the stress ( $\sigma$ ) based on pre-deformation state is expressed by Equation (12).

$$\varepsilon_{eng,T} = \frac{\Delta L'_{0,p}}{L'_0} + \frac{\Delta L_1}{L'_0} \tag{8}$$

$$\varepsilon_{eng,T} = \varepsilon_{eng,BH}^{p} + \frac{\Delta L_1}{\frac{L_1}{L_0 + \Delta L_{0,p}} L_0} = \varepsilon_{eng,BH}^{p} + \left(1 + \varepsilon_{eng,BH}^{p}\right)\frac{\Delta L_1}{L_1} \tag{9}$$

$$\varepsilon_{eng,T} = \left(1 + \varepsilon_{eng,BH}\right) e^{-\frac{S_{BH}\left(1+\varepsilon_{eng,BH}\right)}{E}} e^{\varepsilon_m} - 1 \tag{10}$$

$$\varepsilon_T = \ln\left(\varepsilon_{eng,T} + 1\right) = \varepsilon_{BH} - \frac{S_{BH}\left(1 + \varepsilon_{eng,BH}\right)}{E} + \varepsilon_m \tag{11}$$

$$\sigma = Se^{\varepsilon_T} = Se^{\varepsilon_{BH} - \frac{S\left(1+\varepsilon_{eng,BH}\right)}{E} + \varepsilon_m} \tag{12}$$

## 2.3. Results of Bake Hardening Tensile Tests

Tensile tests of 590DP and 980DP steels were performed on specimens with the pre-strain of 0, 1, 2, 3, 4, 5, 8 and 10 % after baking. The mechanical properties of testing materials are shown in Table 1. The tests were repeated five times for each pre-strain, and the tensile speed was 0.008/s.

Table 1. Mechanical properties of 590DP and 980DP steel

| Material | YS (MPa) | TS (MPa) | Uniform Elongation | Total Elongation |
|---|---|---|---|---|
| 590DP | 391.3 | 642.9 | 0.1873 | 0.2850 |
| 980DP | 636.9 | 989.7 | 0.0943 | 0.1610 |

The engineering stress-strain curves were obtained from experiment according to Equations (9)-(12) regarding the strain and stress, as shown in Figure 8. Stress-strain curves of 590DP steel with respect to the pre-strain shift upper without changing the shape of curve, and the increase of the tensile strength is less than 20 MPa. The yield stress of 980DP steel increases significantly as the yield point elongation occurs. Especially, for the pre-strain of 3 % or more, the upper yield stress becomes the ultimate strength without the uniform elongation, and the stress continuously decreases after the upper yield point. It means that the uniform elongation does not exist, so there is no way to calculate the true stress-strain curve using conventional formulas. Also, the total elongation is not meaningful due to the non-uniform deformation within the gauge section. Overall, the maximum stress tends to increase as the pre-strain increases.

Figure 9 shows the strain distribution before fracture according to the pre-strain of 980DP. Necking is observed up to a pre-strain of 5%, but as the pre-strain increases, the deformation before fracture tends to concentrate in an oblique line. In particular, when the pre-strain is 8% or more, necking is not observed and only

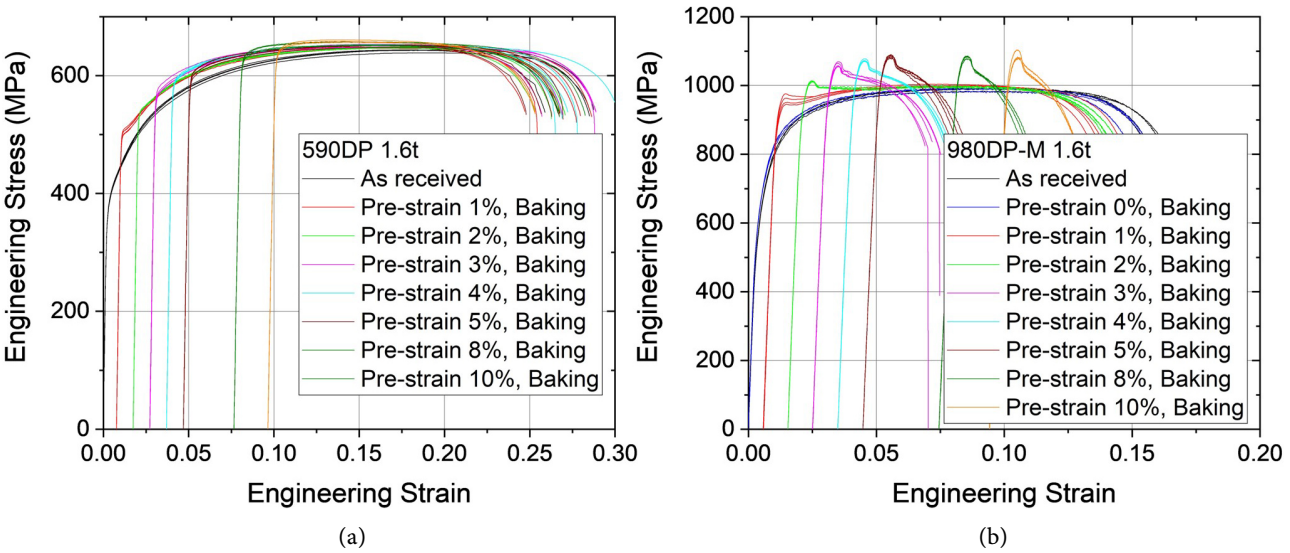


(a) (b)

Figure 8. Engineering stress-strain curves after baking according to pre-strain: (a) 590DP; (b) 980DP.

shear band fracture occurs. In general, Lüders band propagates to the parallel section during yield point elongation, and necking and fracture occur after reaching the ultimate strength. However, when the upper yield stress becomes equal to the maximum stress after baking as the pre-strain increases, the first Lüders band does not propagate and the deformation concentrates on the first band, resulting in shear band fracture. 980DP in Figure 8 and Figure 9 has the maximum stress when the pre-strain is approximately 3% or more, so the shear band deformation becomes dominant.

Figure 10 shows the variation in tensile strength according to the pre-strain. In 590DP steel, the tensile strength gradually increases, and the increase for the pre-strain of 10 % is around 20 MPa. In 980DP, there is no change in tensile strength

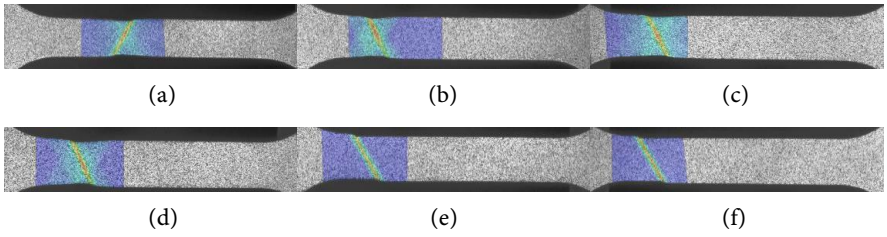


**Figure 9.** Strain distribution of 980DP steel before fracture with respect to the pre-strain: (a) as received; (b) 2 %; (c) 4 %; (d) 5 %; (e) 8 %; (f) 10 %.

when baking without pre-strain, but the tensile strength increases gradually up to the pre-strain of 2 % and then rapidly jumps up to the pre-strain of 4% - 5%. The tensile strength for over the pre-strain of 4% - 5% maintains an almost constant value, and the increase in tensile strength is about 90 MPa, which can sufficiently affect the crash performance of the material.

The increase in strength after baking can be seen as a disadvantage in terms of fracture characteristics. So, tensile tests were performed on various specimens for shear, simple tension, notch and punch bulge, as shown in **Figure 11**, after 5% pre-straining

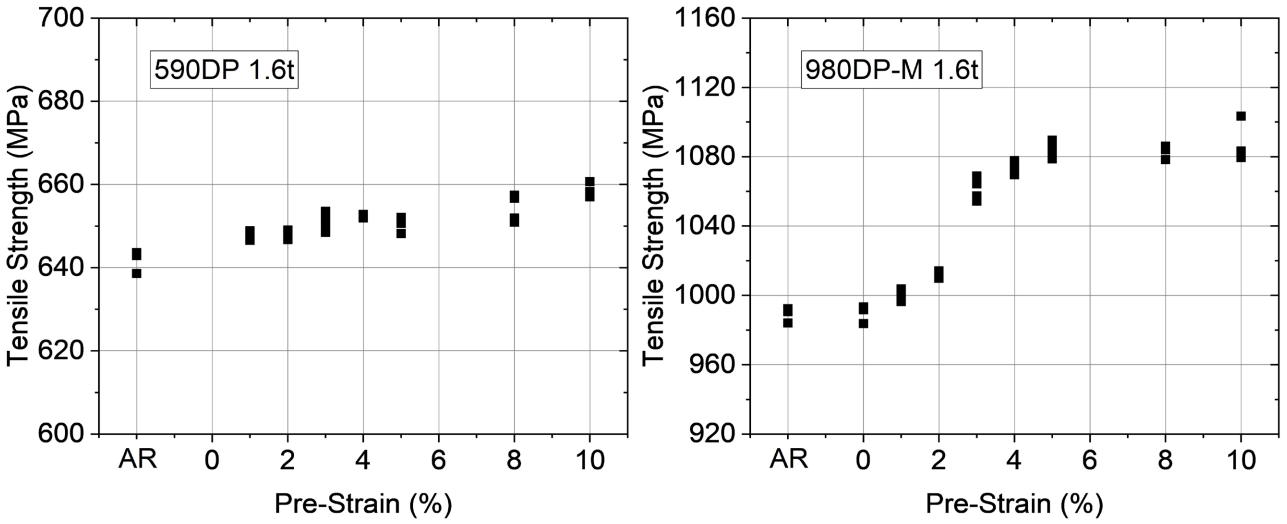


**Figure 10.** Variation of the tensile strength according to pre-straining: (a) 590DP; (b) 980DP.

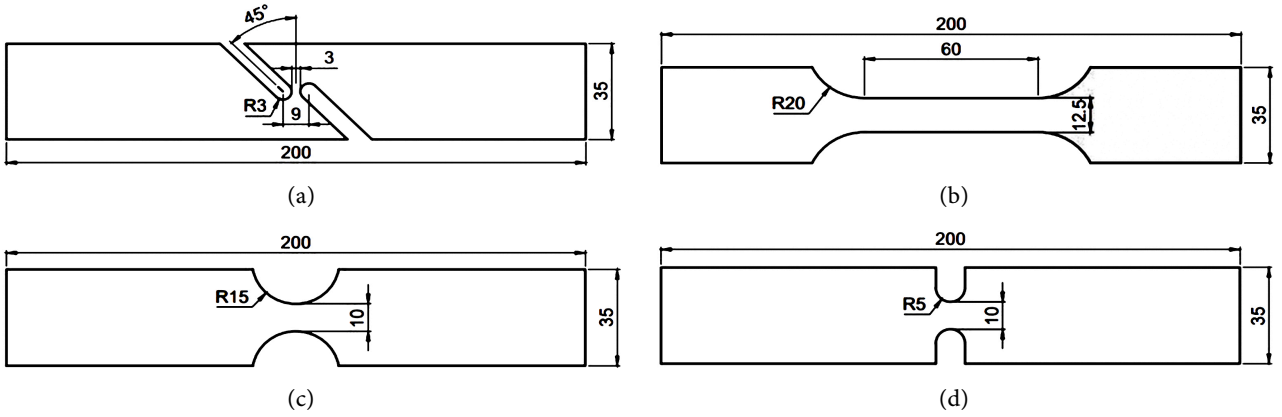

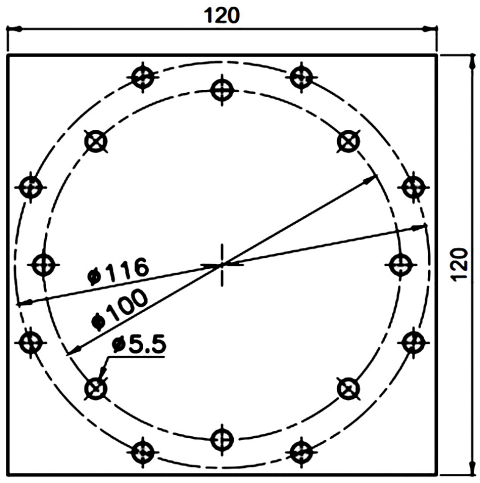


(e)

**Figure 11.** Specimens for the fracture strain: (a) Shear; (b) Simple tension; (c) Notch R15; (d) Notch R5; (e) Punch bulge.

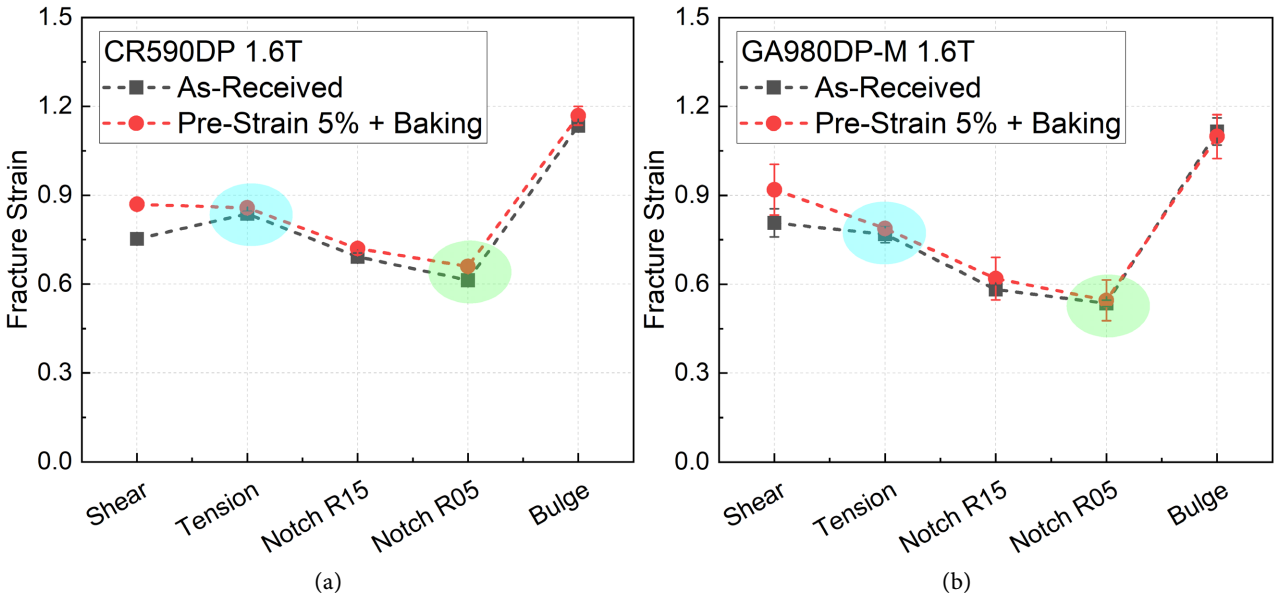


(a) (b)

**Figure 12.** Fracture strain according to pre-straining: (a) 590DP; (b) 980DP.

and baking, and the fracture strain was investigated by DIC system. Overall, the fracture strain remains at similar levels after pre-straining & baking, as shown in **Figure 12**. Especially, the fracture strain shows an equivalent value before and after baking in the bending mode, which is the dominant mode in a crash situation. In conclusion, TS increases and the fracture strain remains equivalent after baking. So, it is going to be beneficial from a crash performance perspective.

## 3. Calculation of True Stress-Strain Curves

### 3.1. DIC Inverse Method for the True Stress-Strain Curve after Reaching the Maximum Load

It is confirmed that the strength of the material generally increased after baking

with pre-straining. Especially, the increase in material strength of UHSS can have a significant effect on the crash performance. Therefore, the change of material properties by forming and baking should be considered in order to enhance the accuracy of crash simulations. The stress-strain curve is required at the crash simulation, so the engineering stress-strain curve in Figure 8 should be converted to true stress-strain curves. However, when the upper yield point is equal to the ultimate strength, as in 980DP steel, there is no way to calculate the true stress-strain curve by formulas.

In this paper, the DIC inverse method was developed to obtain the stress-strain curves about the range after the maximum load from numerical optimization by comparing the force calculated from the strain measured with DIC system with the load-displacement curve.

As shown in Figure 13, the thickness ( $t_i$ ) and the width ( $w_i$ ) under deformation in the small lattice of arbitrary cross-section have the relationship of Equations (13) and (14) with the original thickness ( $t_{o,i}$ ) and the original width ( $w_{o,i}$ ). The volumetric change by the stress in tensile direction is shown in Equation (15) because the tensile test applies stress only in the tensile direction, and there were no stresses in width and thickness directions.

$$t_i = t_{o,i} e^{\varepsilon_{t,i}} \tag{13}$$

$$w_i = w_{o,i} e^{\varepsilon_{w,i}} \tag{14}$$

$$\varepsilon_{x,i} + \varepsilon_{w,i} + \varepsilon_{t,i} = \frac{1-2\nu}{E}\sigma_{x,i} \tag{15}$$

The force ( $f_i$ ) acting on the small lattice of the arbitrary cross-section can be calculated by the tensile stress ( $\sigma_{x,i}$ ), width ( $w_i'$ ), and thickness ( $t_i$ ) of the inclined lattice in Equation (16). Implementing Equations (13) and (14) into Equation (16)

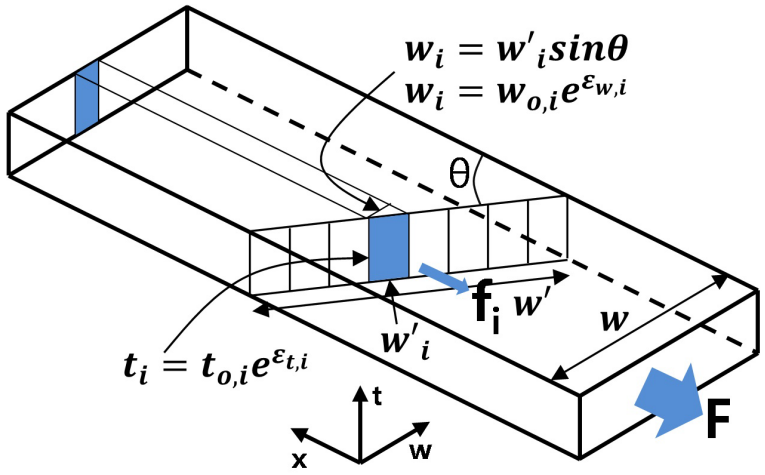


Figure 13. Schematic diagram of an arbitrary cross-section in the parallel section of a tensile specimen.

gives Equation (17). And then, it can be expressed to Equation (18) by inserting Equation (15) to (17).

$$f_i = \sigma_{x,i} t_i w_i' \sin\theta = \sigma_{x,i} t_i w_i \tag{16}$$

$$f_i = \sigma_{x,i} t_{o,i} w_{o,i} e^{\varepsilon_{t,i} + \varepsilon_{w,i}} \tag{17}$$

$$f_i = \sigma_{x,i} t_{o,i} w_{o,i} e^{\frac{1-2\nu}{E}\sigma_{x,i} - \varepsilon_{x,i}} \tag{18}$$

The sum of forces ( $f_i$ ) acting on the small lattice of arbitrary cross-section and the force ($F$) measured in the testing machine is always the same, as shown in Equation (19).

$$F = \sum_i f_i = \sum_i \sigma_{x,i} t_{o,i} w_{o,i} e^{\frac{1-2\nu}{E}\sigma_{x,i} - \varepsilon_{x,i}} \tag{19}$$

If the relationship between stress and strain of a material is known, the force ( $f_i$ ) of the small lattice can be calculated from the strain measured by the DIC system. However, it is not possible to directly calculate the force ( $f_i$ ) of the small lattice because the stress-strain curve is the unknown output that is desired to be obtained in the experiment. Therefore, an optimization method by reducing errors through repetitive calculations called as DIC inverse method was applied to obtain the stress-strain curve. DIC inverse method is that an arbitrary stress-strain curve is assumed, and the stress-strain curve is optimized so that the sum of the calculated forces ( $\sum f_i$ ) using the strain of DIC system becomes equal to the force ($F$) measured by the testing equipment.

Assuming the blue line in Figure 14 as the initial stress-strain curve, the calculated sum of forces ( $\sum f_i$ ) shown in the blue line of Figure 15 is vastly different from the black line of the load data measured in the experiment. When performing optimization by using an in-house optimization program with Excel VBA, the sum of calculated forces is matched precisely with the load-displacement curve in the experiment, as shown in the red line of Figure 15. The final output of the stress-strain curve is the red line in Figure 14. The calculation time is within a few minutes.

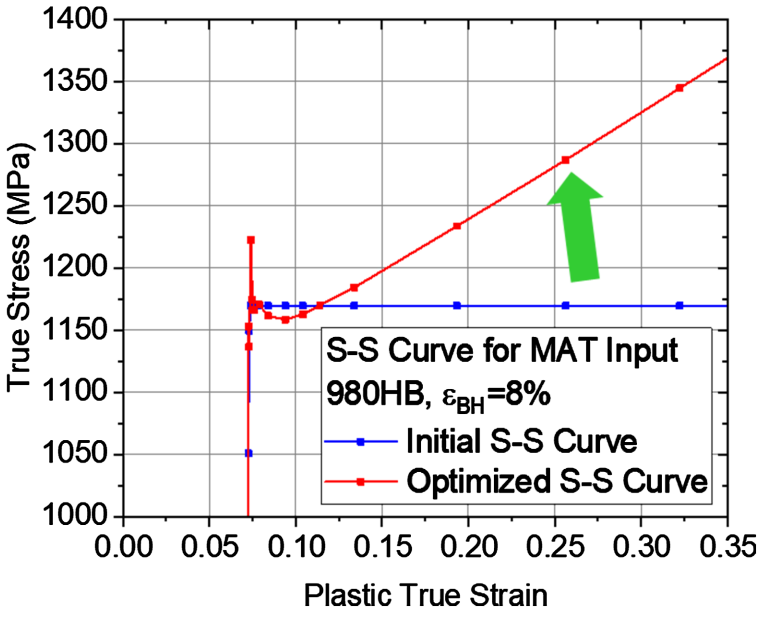


Figure 14. Initial input and optimized stress-strain curves by DIC inverse method.

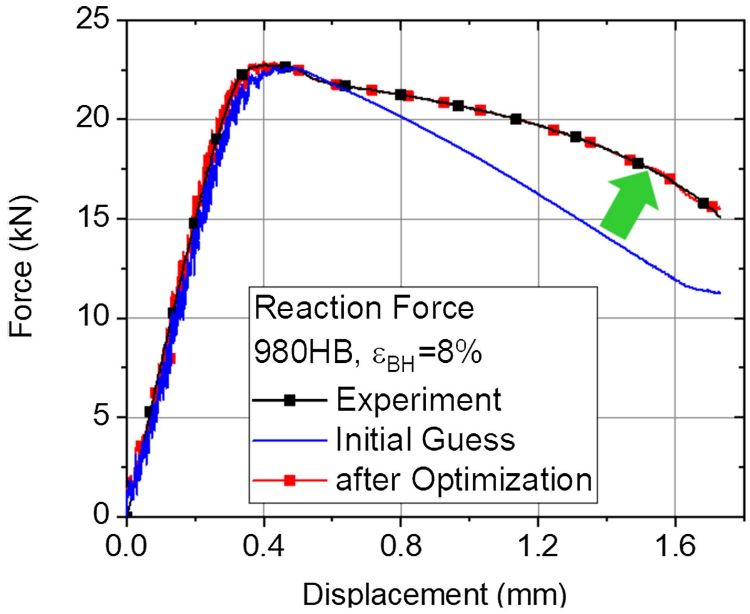


**Figure 15.** Comparison of force-displacement curves between experiment and DIC inverse method.

The advantage of the DIC inverse method is that it can derive a true stress-strain curve through optimization using the strain measured at an arbitrary cross-section. In order to verify the consistency for an arbitrary cross-section, the strain was measured for three cross-sections in the vertical and two diagonal directions in the necking region of the tensile test of 780DP steel, as shown in **Figure 16**, and the true stress-strain curves were derived by applying the DIC inverse method. The lattice size of the cross-section was 0.5 mm regardless of the cross-section direction, and the tensile load applied to the lattice was calculated by multiplying the stress corresponding to the tensile strain by the vertical length and thickness. Therefore, the lattice of the diagonal cross-section has a smaller width in the vertical direction than that in the vertical cross-section. As a result of applying the DIC inverse method, it was confirmed that a consistent true stress-strain curves could be obtained regardless of the cross-section up to a strain of 0.3, as shown in **Figure 17**. Considering that the uniform elongation of 780DP is 0.11, a consistent true stress-strain curve could be obtained up to almost three times the uniform elongation.

The stress obtained by the DIC inverse method is the stress in tensile direction ($\sigma_x$), but the stress in the stress-strain curve is the Von Mises stress. If the two stresses differ, the DIC inverse method can no longer be used. As shown in **Figure 18**, the simulation of the tensile test was performed on a quarter model of the tensile specimen with solid elements, and the difference between $\sigma_x$ and $\sigma_{VM}$ was investigated. As shown in the strain distribution in **Figure 19**, necking occurs in the parallel section after reaching the ultimate strength, and the strain distribution becomes non-uniform in width direction.

The changes in $\sigma_x$ and $\sigma_{VM}$ between the center and the edge are shown in

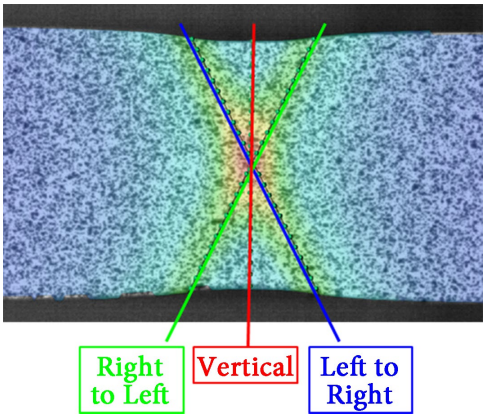


**Figure 16.** Arbitrary sections of necking region of a tensile specimen for measuring the strain for DIC inverse method.

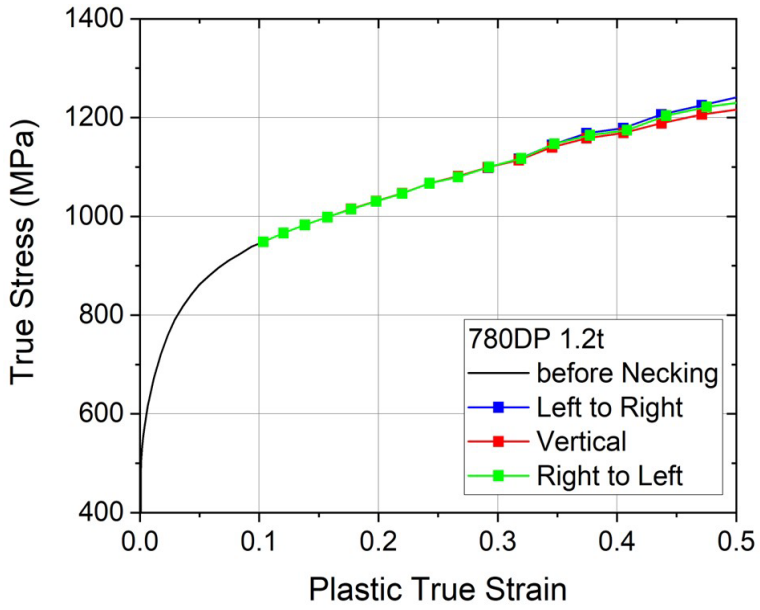


**Figure 17.** True stress-strain curves of 780DP steel obtained from DIC inverse method for arbitrary cross sections.

**Figure 20.** When the deformation in the transverse direction becomes non-uniform after reaching the ultimate strength, $\sigma_x$ and $\sigma_{VM}$ differ. Therefore, it should be considered that the error of the DIC inverse method also increases when local necking occurs. Nevertheless, reliable stress-strain curves can still be obtained by the DIC inverse method in a range of strain that is 2 to 3 times higher than the uniform elongation. Especially, there is an advantage in obtaining stress-strain curves even for cases where uniform elongation is nothing, such as in shear band fracture.

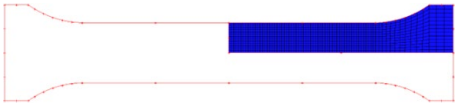

**Figure 18.** 1/4 model of a tensile specimen.

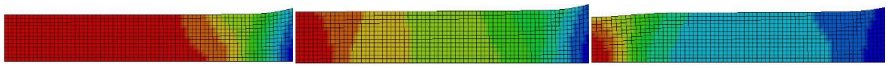

Figure 19. Variation of strain contour after necking.

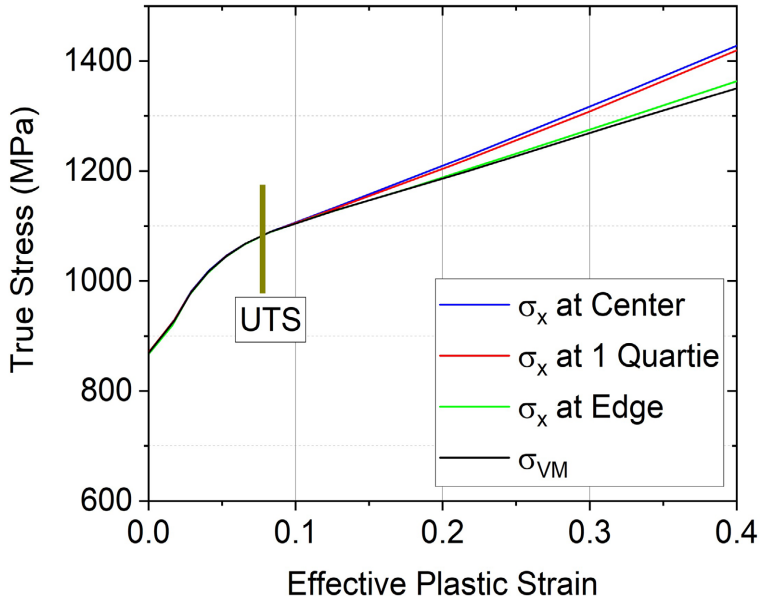


Figure 20. Variation of $\sigma_x$ and Von-Mises stress.

### 3.2. True Stress-Strain Curves of Automotive Steels Considering Forming and Baking Effects

The engineering stress-strain curves of 590DP and 980DP steels in Figure 8 were converted to the true stress-strain curves using the DIC inverse method, as shown in Figure 21. For both materials, oscillations in the true stress-strain curves occur in the strain range of 0.3 or higher, which is thought to be an error resulting from numerical optimization due to noise accompanying strain measurement in DIC. However, the oscillations in the strain range below 0.3 are negligible. 590DP steel, in which no yield point elongation occurs, has a similar shape to the stress-strain curve of the original material after baking. The slope of the stress-strain curve gradually decreases until near the uniform elongation, but after the uniform elongation, it seems to be almost a straight line. On the other hand, 980DP has a yield point elongation in the tensile test after baking. Therefore, the stress in the stress-strain curve sharply decreases after the upper yield point and then increases again. Like 590DP steel, 980DP steel also has an almost straight stress-strain curve after uniform elongation, but the strength increase is significantly greater than that of 590DP steel.

Figure 22 shows the strength increase of the materials after baking compared to the strength of the materials as received at the strain of 0.2. 590DP has a stress increase of less than 20 MPa. The material strength of 980DP increases gradually up to 2% of the pre-strain, but increases rapidly up to 5%. The strength increase for over the pre-strain of 5% maintains an almost constant value, and the increase is about 70 MPa. While the increase of the tensile strength in Figure 10 is 90 MPa, the

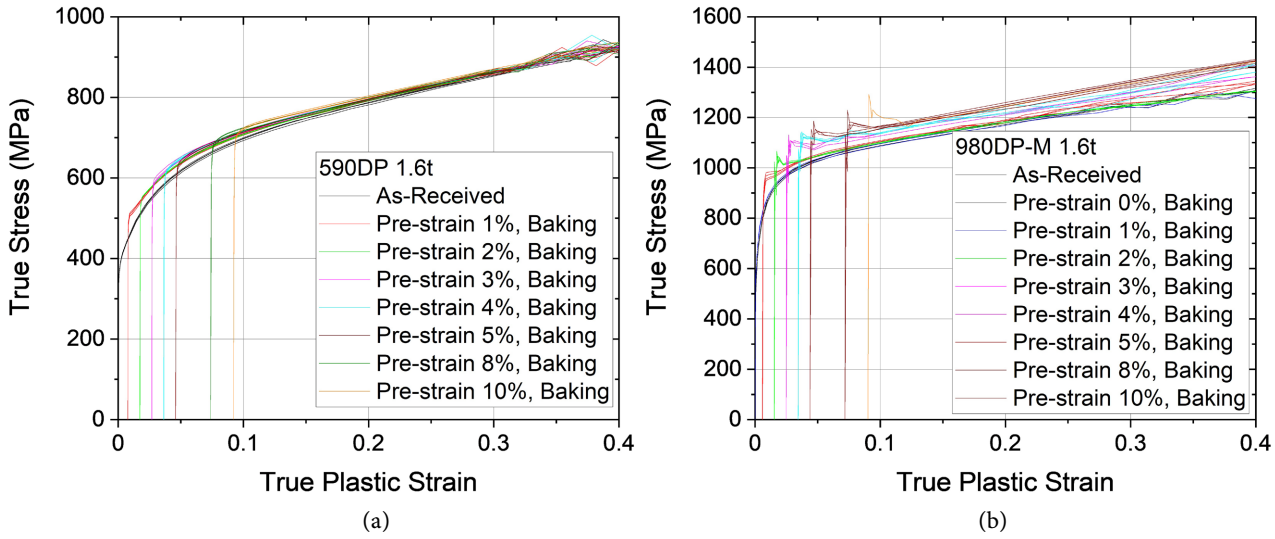


(a) (b)

**Figure 21.** True stress-strain curves after baking according to pre-strain: (a) 590DP; (b) 980DP.

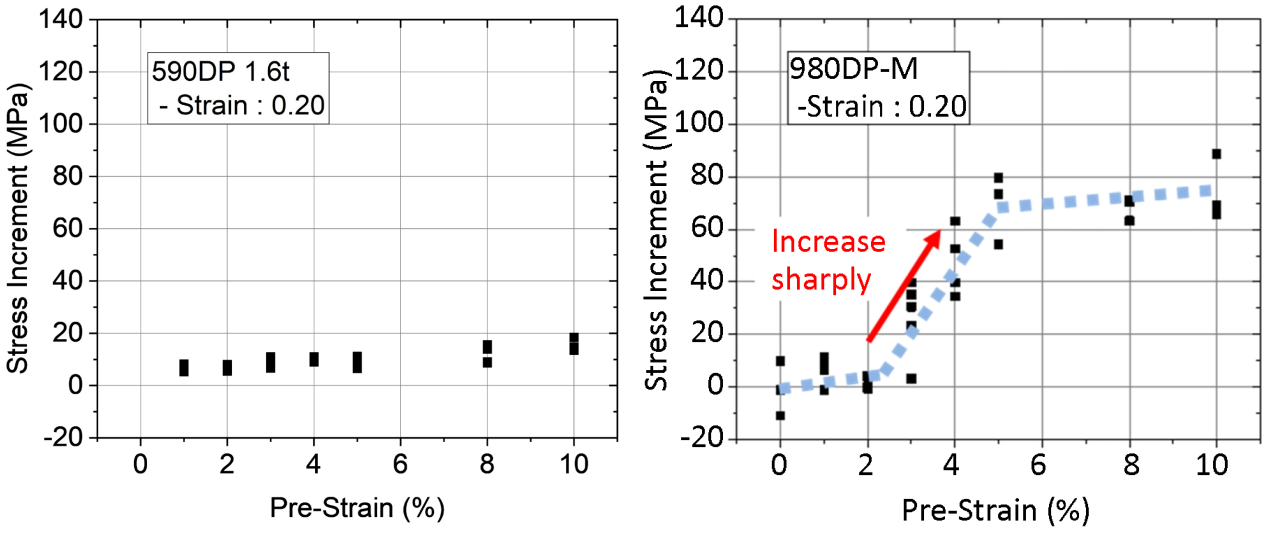


(a) (b)

**Figure 22.** Variation of true stress increment with respect to the pre-strain at strain of 0.2 after baking according to pre-strain: (a) 590DP; (b) 980DP.

increase in material strength for the same strain of 0.2 is 70 MPa and is slightly reduced.

The mechanism of the strength increase by the baking process is related to the Cottrell atmosphere. Cottrell atmosphere involves the interaction between the mobile dislocations and the interstitial atoms, such as carbon inside the ferrite grains. That is, stopping dislocation movement via the Cottrell atmosphere, which is known as strain aging effect, is the mechanism of strengthening. Therefore, the bake hardening depends mainly on the density of the mobile dislocations and the dissolved carbon atoms. Therefore, since 980DP steel has more carbon content than 590DP steel, 980DP steel shows larger strength increase by baking than 590DP steel. There is no change in material strength even if baking is performed without

the pre-strain since there is no change in the density of the mobile dislocation compared to the original material. The density of the mobile dislocation generally increases as pre-strain increases, but there is obvious saturation limit of the dislocation density for excessive pre-strain. 980DP steel has a limit to the strength increase at pre-strain of 5% or more, which is related to the limit of the increase in dislocation density.

## 4. Simulation Method Considering Effects of Forming and Baking

### 4.1. Work Hardening Model to Describe Effects of Baking According to Pre-Strain

A suitable work hardening model is required to apply the stress-strain curve in Figure 21 into simulation as material properties. Therefore, this study proposed a mathematical work hardening model based on experimental data. The material strength variation by baking can be divided into a drastic decrease after the peak stress in yield point elongation and an increase in the overall work hardening curve, as shown in Figure 23. It is classified into the work hardening curve of the original material ( $\sigma_{AR}$ ), the increase in the work hardening curve by baking ( $\Delta\sigma_{Shift}$ ), and the initial stress increase by yield point elongation ( $\Delta\sigma_{Peak}$ ), as shown in Figure 24, and is expressed as in Equation (12). Any hardening model can be used for the base work hardening curve ( $\sigma_{AR}$ ), including Swift-Voce of Equation (21), Hockett-Sherby of Equation (22), Piecewise linear data, etc.

$$\sigma = \sigma_{AR}(\varepsilon) + \Delta\sigma_{Shift} + \Delta\sigma_{Peak} \tag{20}$$

$$\sigma = \alpha C_1 \left(C_2 + \varepsilon_p\right)^{C_3} + (1-\alpha)\left(C_4 + (C_5 - C_4)\mathrm{e}^{-C_6\varepsilon_p}\right) \tag{21}$$

$$\sigma = C_2 - (C_2 - C_1)\mathrm{e}^{-C_3\varepsilon_p{}^{C_4}} \tag{22}$$

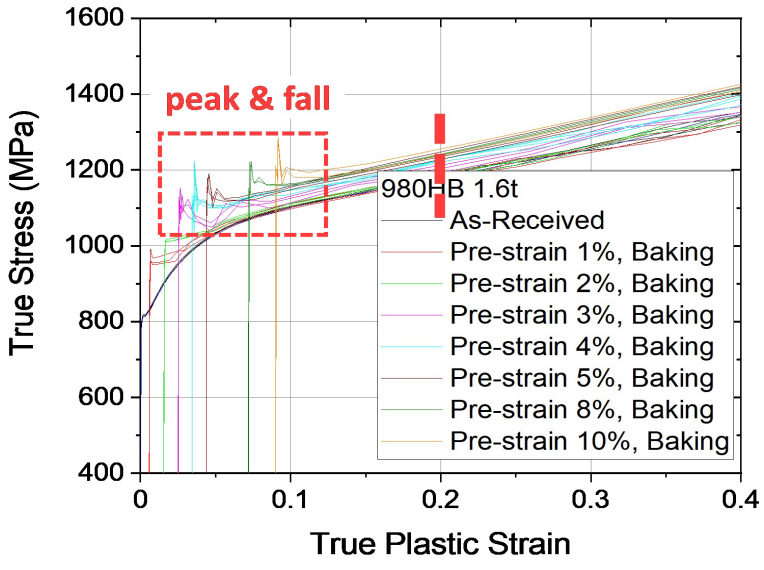


Figure 23. Analysis of stress variation with respect to the pre-strain.

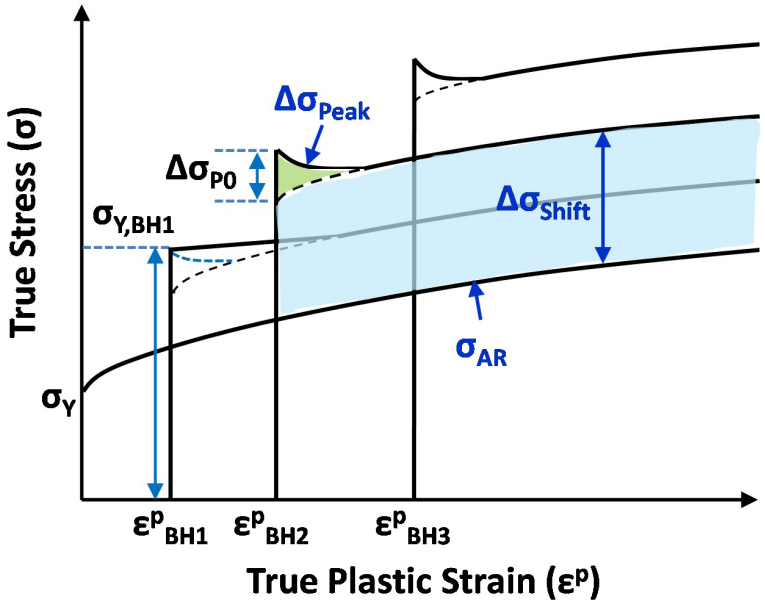


**Figure 24.** Classification of stress in stress-strain curve after pre-strain and baking.

As shown in Figure 22(b), the strength increase has a transition zone about the pre-strain of 3% - 5% in which the strength increases rapidly. In order to describe this tendency of the strength increase by baking ( $\Delta\sigma_{Shift}$ ), Boltzmann sigmoidal function in Equation (23) is adopted. As shown in Figure 25, Boltzmann sigmoidal function is characterized by a plateau of bottom ( $y_1$ ) and top ( $y_2$ ) with an inflection point ( $x_0$ ) value describing the point where the $x$-value is exactly between the bottom and top values and a coefficient ($\kappa$) indicating the slope of the transition zone.

$$y = y_1 + \frac{y_2 - y_1}{1 + e^{\frac{x_0 - x}{\kappa}}} \tag{23}$$

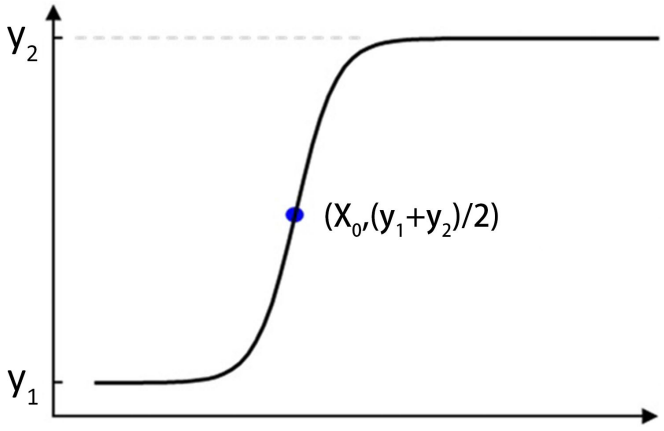


**Figure 25.** Boltzmann sigmoidal function.

The top and bottom values of Boltzmann sigmoidal function are constant, but

the material strength against the pre-strain in the experiment changes slightly at top and bottom, as shown in Figure 22(b). Therefore, the top and bottom in new hardening model were assumed as linear functions of Equations (25) and (26). The strength increase by baking ( $\Delta\sigma_{Shift}$ ) is expressed in Equation (24) with bottom of the strength increase ( $\sigma_{\Delta,min}$ ), top of the strength increase ( $\sigma_{\Delta,max}$ ), the inflection of pre-strain ( $\varepsilon_{tran1}$ ) and the slope coefficient of transition zone ( $\kappa_1$ ). In order not to exaggerate the strength change in sections beyond the pre-strain evaluated in the experiment, the maximum value of the pre-strain ( $\varepsilon_{BH,Max}$ ) could be set. Coefficients *a*, *b*, *c* and *d* are defined to describe the change in the material strength at top and bottom.

$$\Delta\sigma_{Shift} = \sigma_{\Delta,min} + \frac{\sigma_{\Delta,max} - \sigma_{\Delta,min}}{1+\mathrm{e}^{\frac{\varepsilon_{tran1} - \min\left(\varepsilon_{BH}^{p}, \varepsilon_{BH,Max}\right)}{\kappa_1}}} \tag{24}$$

$$\sigma_{\Delta,min} = a + b\min\left(\varepsilon_{BH}^{p}, \varepsilon_{BH,Max}\right) \tag{25}$$

$$\sigma_{\Delta,max} = c + d\min\left(\varepsilon_{BH}^{p}, \varepsilon_{BH,Max}\right) \tag{26}$$

Even if baking is applied after pre-straining, the yield point elongation does not always occur in all materials. In 590DP steel, the yield point elongation does not occur regardless of the amount of pre-strain, but in 980DP steel, yield point elongation may occur when pre-strain exceeds a certain level. The Boltzmann function was also applied to express the yield point elongation that occurs after a certain level of pre-strain. When the yield point elongation occurs, the stress decreases rapidly as the strain increases after reaching the upper yield point. New hardening model applied an exponential function to describe rapid stress reduction. Because the amount of stress increase at the upper yield point varies depending on the pre-strain, an exponential function was adopted. Summarizing the above explanation, the initial stress increase by yield point elongation ( $\Delta\sigma_{Peak}$ ) is expressed in Equations (27) and (28). $\varepsilon_{tran2}$ and $\kappa_2$ are coefficients related to the inflection of pre-strain and the slope coefficient of the transition zone about occurrence of the yield point elongation, respectively. $K_{BH}$, $\varepsilon_{B0}$ and *m* are coefficients about the stress increase at the upper yield point.

$$\Delta\sigma_{Peak} = \frac{1}{1+\mathrm{e}^{\frac{\varepsilon_{tran2} - \min\left(\varepsilon_{BH}^{p}, \varepsilon_{BH,Max}\right)}{\kappa_2}}} \Delta\sigma_{p0}\mathrm{e}^{-\frac{\varepsilon^{p} - \min\left(\varepsilon_{BH}^{p}, \varepsilon_{BH,Max}\right)}{t_1}} \tag{27}$$

$$\Delta\sigma_{p0} = K_{BH}\left(\varepsilon_{B0} + \min\left(\varepsilon_{BH}^{p}, \varepsilon_{BH,Max}\right)\right)^{m} \tag{28}$$

Combining Equations (20), (24) and (27) leads to Equation (29). The basic requirement of the work hardening model is that it must be differentiable with respect to the strain. The strength increase by baking ( $\Delta\sigma_{Shift}$ ) in Equation (24) is constant to the strain. Therefore, the new work hardening model considering forming and baking is differentiable, and the differentiation is expressed with Equation (30).

$$\sigma = \sigma_{AR} + \sigma_{\Delta,min} + \frac{\sigma_{\Delta,max} - \sigma_{\Delta,min}}{1+\mathrm{e}^{\frac{\varepsilon_{tran1} - \min\left(\varepsilon_{BH}^{p}, \varepsilon_{BH,Max}\right)}{\kappa_1}}} + \frac{1}{1+\mathrm{e}^{\frac{\varepsilon_{tran2} - \min\left(\varepsilon_{BH}^{p}, \varepsilon_{BH,Max}\right)}{\kappa_2}}} \Delta\sigma_{p0} \mathrm{e}^{-\frac{\varepsilon^{p} - \min\left(\varepsilon_{BH}^{p}, \varepsilon_{BH,Max}\right)}{t_1}} \tag{29}$$

$$\frac{\mathrm{d}\sigma}{\mathrm{d}\varepsilon^{p}} = \frac{\mathrm{d}\sigma_{AR}}{\mathrm{d}\varepsilon^{p}} - \frac{1}{t_1} \frac{1}{1+\mathrm{e}^{\frac{\varepsilon_{tran2} - \min\left(\varepsilon_{BH}^{p}, \varepsilon_{BH,Max}\right)}{\kappa_2}}} \times K_{BH}\left(\varepsilon_{B0} + \min\left(\varepsilon_{BH}^{p}, \varepsilon_{BH,Max}\right)\right)^{m} \mathrm{e}^{-\frac{\varepsilon^{p} - \min\left(\varepsilon_{BH}^{p}, \varepsilon_{BH,Max}\right)}{t_1}} \tag{30}$$

Because the new model has 13 coefficients, the coefficient derivation procedure is somewhat complicated. In this paper, the coefficients were derived using an in-house program. The coefficients of the new work hardening model considering pre-strain and baking are listed in Table 2. 590DP and 980DP steels are fitted by the new work hardening model and compared with the experimental data, as shown in Figure 26. Both 590DP without yield point elongation and 980DP with yield point elongation are well described by the new work hardening model.

**Table 2.** Coefficients of new work hardening model for 590DP and 980DP.

| Material | THK (mm) | $a$ (MPa) | $b$ (MPa) | $c$ (MPa) | $d$ (MPa) | $\kappa_1$ | $\varepsilon_{tran1}$ | $K_{BH}$ (MPa) | $\varepsilon_{B0}$ | $m$ | $t_1$ | $\kappa_2$ | $\varepsilon_{tran2}$ |
|---|---|---|---|---|---|---|---|---|---|---|---|---|---|
| 590DP | 1.6 | 5.21 | 0 | 0 | 0 | 0.0086 | 0.288 | 10.84 | 0.1348 | −0.525 | 0.079 | 0.001 | −0.0414 |
| 980DP | 1.6 | −4.1 | 0 | 67.9 | 0 | 0.0059 | 0.0288 | 10.99 | 6.7E−05 | −0.514 | 0.017 | 0.001 | 0.0035 |

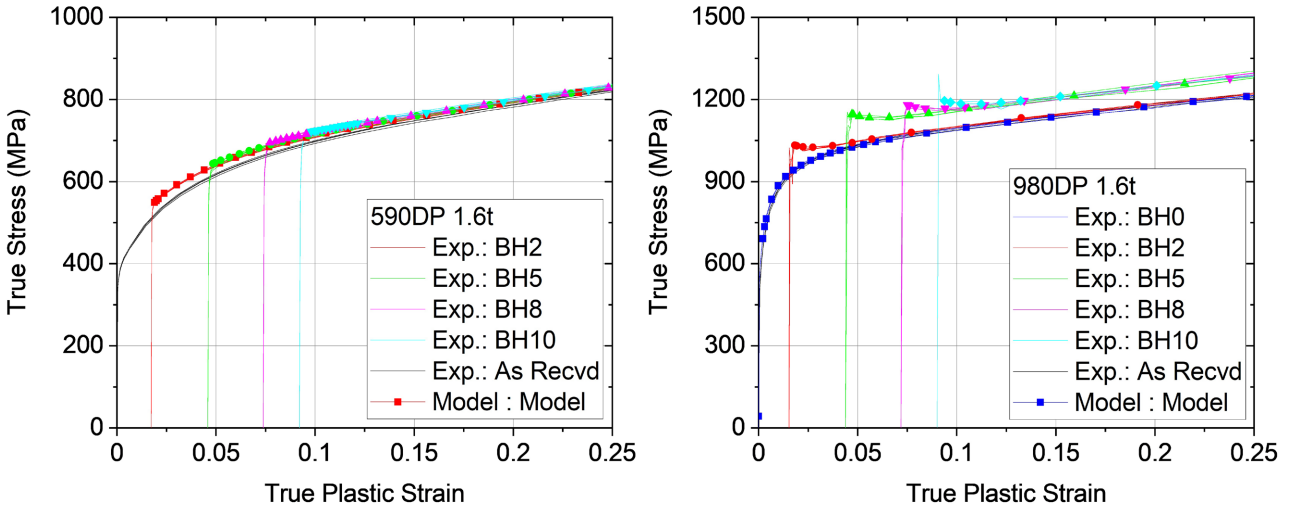


(a) (b)

**Figure 26.** Comparison of the new hardening model for BH and experiment: (a) 590DP; (b) 980DP.

### 4.2. Validation of the New Model Using LS-Dyna User Material Subroutine

The newly proposed work hardening model considering pre-deformation and baking was constructed and verified as LS-Dyna user material subroutine. As the first benchmark test, simple tension was performed with quarter model in Figure 27. If the pre-strain is not constant in longitudinal direction, necking happens at the beginning of the tension, and it is difficult to verify the baking effect. Therefore, the pre-strain was kept constant in longitudinal direction, and pre-strains of 0.01 and 0.05 were applied on top and bottom, respectively. Figure 28 shows the stress-strain curves using the new work hardening model for 590DP with pre-strains of 0, 0.01, 0.03, 0.05, and 0.1 in the benchmark test.

When the test model is tensioned with uniform velocity in *x*-direction, the stress and the strain at elements 7 and 8 were measured and compared with input material properties. As a result of the analysis, it was confirmed that the input stress-strain curve and its simulation matched exactly, as shown in Figure 29, thereby verifying that the user material subroutine was constructed well.

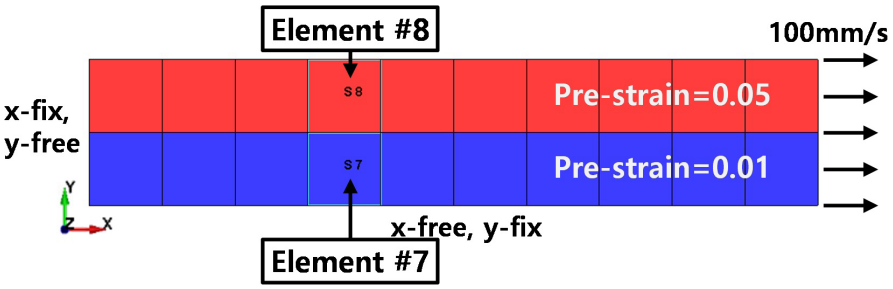


Figure 27. FE model of benchmark test for simple tension.

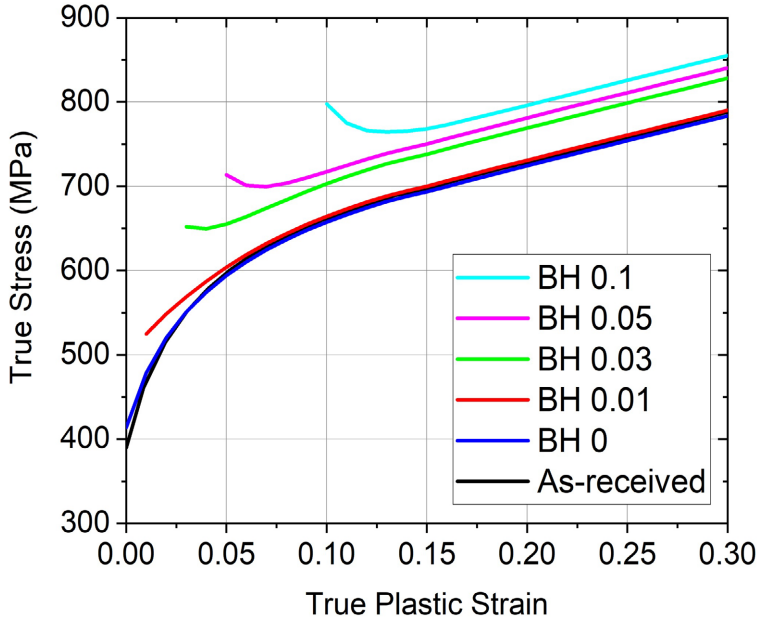


Figure 28. Stress-strain curves of 590DP steel from new model for BH.

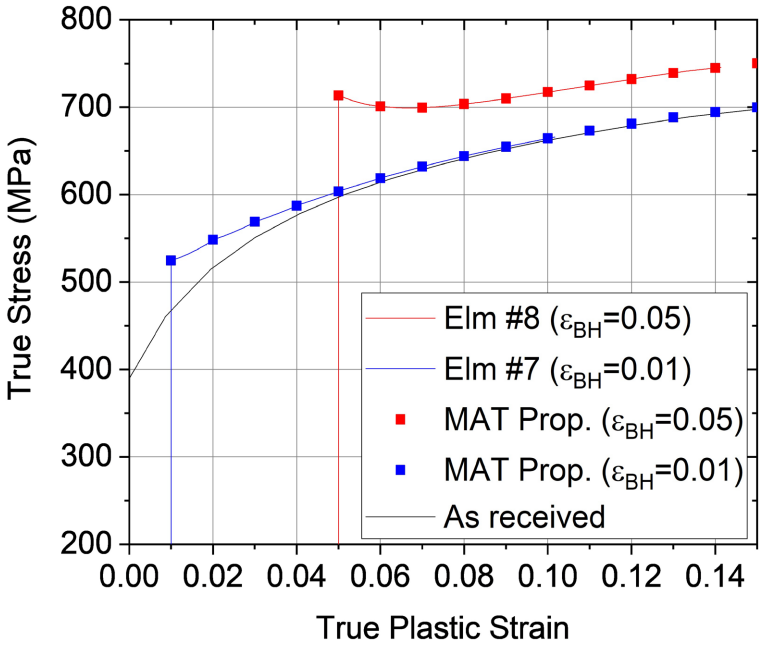


**Figure 29.** Comparison of stress-strain curves of simulation with input hardening model.

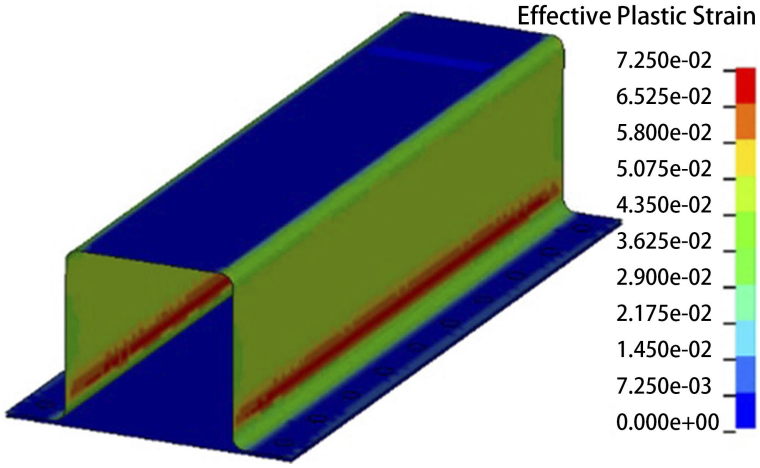


**Figure 30.** Contour of pre-strain in single hat specimen.

In order to confirm the effect of strength increase by forming and baking, the simulation of axial crush of a hat specimen in **Figure 30** was performed. The thickness reduction on the wall by about 5% was generated by forming simulation. The spot weld fracture was not considered. One side was fixed and the other side was collapsed vertically at constant velocity. Compared to the original material, the case that considered both work hardening and bake hardening, showed the greatest load and energy absorption, as shown in **Figure 31**. The energy absorption of the case considering both work hardening and bake hardening was approximately 5% larger than that of the case considering only work hardening. This difference is a significant level in crash performance. Therefore, it is necessary to apply the bake hardening according to the pre-strain as well as work hardening in order to

accurately predict the crashworthiness.

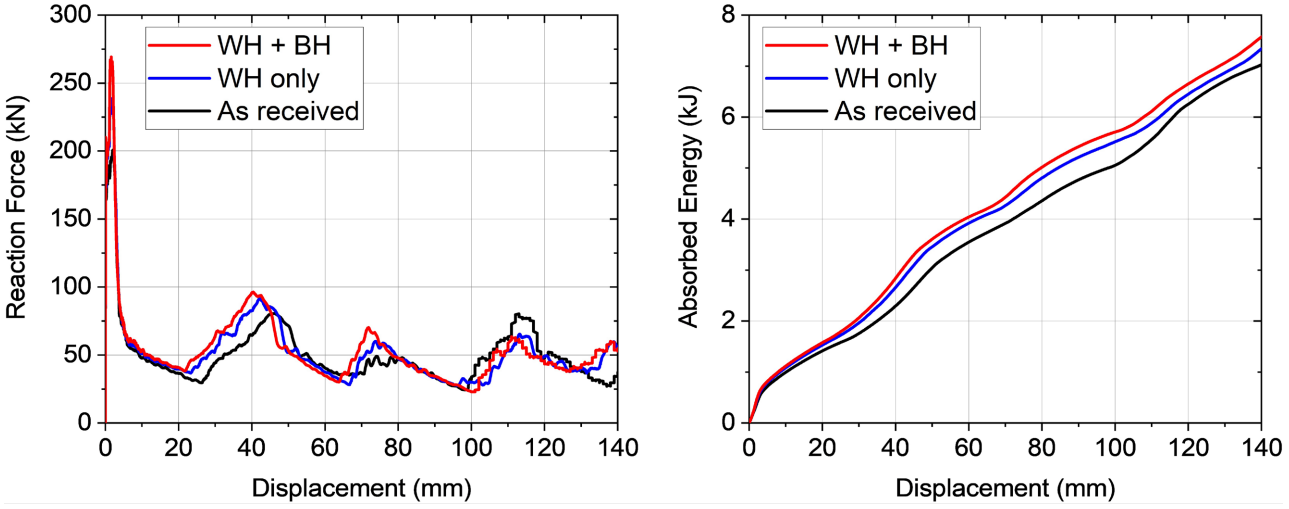


(a) (b)

**Figure 31.** Effects of consideration of work hardening and bake hardening in the axial crash of single hat specimen on: (a) Force-displacement curve; (b) Absorbed energy.

## 5. Conclusions

To consider the change of material properties by work hardening of the forming process and bake hardening of the painting process in crash analysis, a bake hardening test method and work hardening model were developed.

In order to prevent the fracture outside an extensometer of a tensile specimen caused by the difference in bake hardening due to the non-uniform pre-strain, the tensile specimen was re-machined from the parallel section of a large specimen to which the pre-strain was applied and re-tensioned it. When baking after pre-deformation, UHSS usually exhibits the yield point elongation, and the upper yield point reaches the tensile strength without the uniform elongation as the pre-strain increases. Therefore, it is impossible to calculate the true stress-strain curve by a conventional formula. In this study, it was developed the DIC inverse method to obtain the stress-strain curve by comparing the force calculated from the local strain measured by DIC system with force-displacement curve from a test. Stress-strain curves of 590DP and 980DP steels were derived using the DIC inverse method.

A novel work hardening model was developed to apply the change in the stress-strain curve according to pre-strain and baking into simulation. The model is expressed as the sum of the terms for the work hardening curve of the original material, the increase in strength due to baking, and the increase in initial stress due to yield point elongation. In order to apply the new work hardening model to the simulation, an LS-Dyna user material subroutine was constructed and verified by a benchmark test of a simple tensile specimen. In the axial crush of a hat specimen, considering both work hardening and bake hardening showed a significant difference in crash performance compared to only considering work hardening. Therefore,

it is necessary to consider bake hardening according to forming history for an accurate prediction of the crash analysis.

## Conflicts of Interest

The authors declare no conflicts of interest regarding the publication of this paper.

## References

[1] Badkoobeh, F., Nouri, A. and Hassannejad, H. (2020) The Bake Hardening Mechanism of Dual-Phase Silicon Steels under High Pre-Strain. *Materials Science and Engineering*: *A*, **770**, Article ID: 138544. https://doi.org/10.1016/j.msea.2019.138544

[2] Ramazani, A., Bruehl, S., Gerber, T., Bleck, W. and Prahl, U. (2014) Quantification of Bake Hardening Effect in DP600 and TRIP700 Steels. *Materials & Design*, **57**, 479-486. https://doi.org/10.1016/j.matdes.2014.01.001

[3] Soliman, M. and Palkowski, H. (2020) Tensile Properties and Bake Hardening Response of Dual Phase Steels with Varied Martensite Volume Fraction. *Materials Science and Engineering*: *A*, **777**, Article ID: 139044. https://doi.org/10.1016/j.msea.2020.139044

[4] Chaurasiya, R., Mukhopadhyay, G. and Maji, P. (2024) Effect of Prestrain on Tensile Behavior of HS800 Steel Sheet. *Materials Today Communications*, **38**, Article ID: 108047. https://doi.org/10.1016/j.mtcomm.2024.108047

[5] Robertson, L., Hilditch, T. and Hodgson, P. (2008) The Effect of Prestrain and Bake Hardening on the Low-Cycle Fatigue Properties of TRIP Steel. *International Journal of Fatigue*, **30**, 587-594. https://doi.org/10.1016/j.ijfatigue.2007.06.002

[6] Pereloma, E.V., Russell, K.F., Miller, M.K. and Timokhina, I.B. (2008) Effect of Pre-Straining and Bake Hardening on the Microstructure of Thermomechanically Processed CMnSi TRIP Steels with and without Nb and Mo Additions. *Scripta Materialia*, **58**, 1078-1081. https://doi.org/10.1016/j.scriptamat.2008.02.002

[7] Stoughton, T., Yoon, J., Min, J. and Carsley, J. (2019) A DIC Technological Revolution. 12*th Forming Technology Forum*, Herrsching, 19-20 September 2019.

[8] Coppieters, S., Cooreman, S., Sol, H., Van Houtte, P. and Debruyne, D. (2011) Identification of the Post-Necking Hardening Behaviour of Sheet Metal by Comparison of the Internal and External Work in the Necking Zone. *Journal of Materials Processing Technology*, **211**, 545-552. https://doi.org/10.1016/j.jmatprotec.2010.11.015

[9] Zhao, K., Wang, L., Chang, Y. and Yan, J. (2016) Identification of Post-Necking Stress-Strain Curve for Sheet Metals by Inverse Method. *Mechanics of Materials*, **92**, 107-118. https://doi.org/10.1016/j.mechmat.2015.09.004

[10] Capilla, G., Hamasaki, H. and Yoshida, F. (2017) Determination of Uniaxial Large-Strain Workhardening of High-Strength Steel Sheets from In-Plane Stretch-Bending Testing. *Journal of Materials Processing Technology*, **243**, 152-169. https://doi.org/10.1016/j.jmatprotec.2016.12.002

[11] Ballarin, V., Soler, M., Perlade, A., Lemoine, X. and Forest, S. (2009) Mechanisms and Modeling of Bake-Hardening Steels: Part I. Uniaxial Tension. *Metallurgical and Materials Transactions A*, **40**, 1367-1374. https://doi.org/10.1007/s11661-009-9813-5

[12] Durrenberger, L., Lemoine, X. and Molinari, A. (2011) Effects of Pre-Strain and Bake-Hardening on the Crash Properties of a Top-Hat Section. *Journal of Materials Processing Technology*, **211**, 1937-1947. https://doi.org/10.1016/j.jmatprotec.2011.06.015

[13] Schwab, R. and Ruff, V. (2013) On the Nature of the Yield Point Phenomenon. *Acta*

*Materialia*, **61**, 1798-1808. https://doi.org/10.1016/j.actamat.2012.12.003

[14] Riemensperger, D. (2016) Considering Bake Hardening for Deformed Sheet Steel. *German LS-DYNA Forum*, Bamberg, 10-12 October 2016.

[15] Koch, D., Andrade, F., Haufe, A. and Feucht, M. (2018) Bake-Hardening Effect in Dual-Phase Steels Experimental and Numerical Investigation. 15*th International LS-DYNA Users Conference*, Dearbonn, MI, 10-12 June 2018, 1-10.

[16] Thuillier, S., Zang, S., Troufflard, J., Manach, P. and Jegat, A. (2018) Modeling Bake Hardening Effects in Steel Sheets—Application to Dent Resistance. *Metals*, **8**, Article 594. https://doi.org/10.3390/met8080594